Short-Range n-p Correlations from ^{12}C(p,2p + n) at 6 to 9 GeV/c Beam Momentum

J. W. Watson[a] for the EVA Collaboration

A. Tang[a], J. Aclander[b], J. Alster[b], G. Asryan[d,c], Y. Averichev[h], D. Barton[d], V. Baturin[f,e], N. Bukhtoyarova[d,e], A. Carroll[d], S. Gushue[d], S. Heppelmann[f], A. Leksanov[f], Y. Makdisi[d], A. Malki[b], E. Minina[f], I. Navon[b], H. Nicholson[g], A. Ogawa[f], Yu. Panebratsev[h], E. Piasetzky[b], A. Schetkovsky[f,e], S. Shimanskiy[h], D. Zhalov[f]

[a] *Dept. of Physics, Kent State Univ., Kent, OH 44242, U.S.A.*

[b] *School of Physics and Astronomy, Sackler Faculty of Exact Sciences, Tel Aviv University, Ramat Aviv 69978, Israel*

[c] *Yerevan Physics Institute, Yerevan 375036, Armenia*

[d] *Collider-Accelerator Department, Brookhaven National Laboratory, Upton, NY 11973, USA*

[e] *Petersburg Nuclear Physics Institute, Gatchina, St. Petersburg 188350, Russia*

[f] *Physics Department, Pennsylvania State University, University Park, PA 16801, U.S.A.*

[g] *Dept. of Physics, Mount Holyoke College, South Hadley, MA 01075, U.S.A.*

[h] *J.I.N.R., Dubna, Moscow 141980, Russia*

We studied the ^{12}C(p,2p+n) reaction at beam momenta of 5.9, 8.0 and 9.0 GeV/c. For quasielastic (p,2p) events we reconstructed $\mathbf{p}_f$, the momentum of the knocked-out proton before the reaction; $\mathbf{p}_f$ was then compared (event-by-event) with $\mathbf{p}_n$, the measured, coincident neutron momentum. For $|\mathrm{p}_n| > \mathrm{k}_F = 0.220$ GeV/c (the Fermi momentum) a strong back-to-back directional correlation between $\mathbf{p}_f$ and $\mathbf{p}_n$ was observed, indicative of short-range n-p correlations. From $\mathbf{p}_n$ and $\mathbf{p}_f$ we constructed the distributions of c.m. and relative motion in the longitudinal direction for correlated pairs. After correcting for detection efficiency, flux attenuation and solid angle, we determined that 49 ± 13 % of events with $|\mathrm{p}_f| > \mathrm{k}_F$ had directionally correlated neutrons with $|\mathrm{p}_n| > \mathrm{k}_F$. Thus short-range 2N correlations are a major source of high-momentum nucleons in nuclei.

I. INTRODUCTION

For the past half century, the dominant model for the structure of nuclei, especially light nuclei, has been the nuclear shell model. In the shell model, the long-range (∼ 2 fm) part of the NN interaction, in combination with the Pauli principle, produces an average potential in which the nucleons undergo nearly independent motion, and the residual interactions can be treated by perturbation theory. However the NN interaction is also highly repulsive at short-range (∼ 0.4 fm). This short-range two-nucleon repulsion is responsible for the saturation density of nuclei, e.g. the nearly constant density in the interior of all stable nuclei heavier than ^{4}He. The effect of this two-nucleon short-range (2N-SRC) repulsion should also manifest itself in the motions of the nucleons in the nucleus. In 1998, Y. Mardor et al. [1] showed that for high-energy (p,2p) reactions at high momentum transfer, quasi-elastic scattering can be identified. They also showed, assuming the validity of the Plane-Wave Impulse Approximation (PWIA), that high-momentum-transfer (p,2p) yields the same momentum distributions as (e,e′p). Building on this result, Aclander et al. [2] described a new technique for observing 2N-SRC with a high-momentum-transfer proton reaction, based on a proposal by Frankfurt and Strikman [3]. In a recent publication [4] we demonstrate that 2N-SRC can be observed directly and that their contribution to quasi-elastic scattering is sizable at high initial momentum. We also presented the first measured results of the c.m. momentum of the correlated NN pair as well as the relative momentum of the two nucleons in their c.m. frame. This topic has also been actively pursued in recent years with electrons at lower momentum transfer [5–7].

For quasi-elastic knockout of protons from nuclei, e.g. ^{12}C(p,2p) in [1,2] and for this work, we can reconstruct (event-by-event) the three momentum $\mathbf{p}_f$ that the struck target proton had before the reaction:

$$\mathbf{p}_f = \mathbf{p_1} + \mathbf{p_2} - \mathbf{p_0} \tag{1}$$

where $\mathbf{p}_0$ is the momentum of the incident proton and $\mathbf{p}_1$ and $\mathbf{p}_2$ are the momenta of the two detected protons. Note that our analysis is based on the assumption that the PWIA is valid, an assumption verified at the level of a few percent for our experimental conditions [1]. The question we then ask is whether or not there is a coincident neutron with $\mathbf{p}_n \approx -\mathbf{p}_f$. To answer this question, we deployed 36 neutron detectors to look for triple coincidences of the kind ^{12}C(p,2p+n). We have already published a report on the inclusive neutron spectra [8]. In this paper we report on the momentum correlations.

The data presented in this paper were taken with the EVA spectrometer at the Alternating Gradient Synchrotron at Brookhaven National Laboratory. The EVA spectrometer was designed for studying quasi-elastic (p,2p) reactions near 90° c.m. to investigate nuclear transparency [9]. For p-p elastic scattering near 90°, the cross section $\frac{d\sigma}{dt}$ falls as s^{-10} where s and t are the standard Mandelstam variables. This s^{-10} dependence is consistent with constituent quark counting rules for hard reactions at momenta of several GeV/c and up. From this strong dependence on s we expect p-p quasi-elastic scattering to occur preferentially with nuclear protons that have the longitudinal component of $\mathbf{p}_f$ in the beam direction, because this reduces s and increases $\frac{d\sigma}{dt}$ [10]. When two nucleons in a nucleus interact at short range, they must have large, nearly equal, momenta in opposite directions (because of their strong repulsion at short range) [11]. If the pair is broken by a quasi-elastic interaction one of the nucleons may emerge from the nucleus, with relatively large momentum, in a direction opposite to original momentum of its partner. Our experiment then consists of measuring the two protons of the quasi-elastic scattering in triple coincidence with the emerging correlated neutron. Since $\mathbf{p}_f$ should have a large component parallel to the beam, we placed 36 neutron detectors primarily in the backward hemisphere, to search for neutrons with $\mathbf{p}_n \approx -\mathbf{p}_f$. In Sect. II of this paper we describe the experimental setup. In Sect. III we present our triple-coincidence (p,2p+n) results, and study the directional correlation between $\mathbf{p}_n$ and $\mathbf{p}_f$. In Sect. IV we extract the relative and c.m. motion for correlated pairs. In Sect. V, for quasi-elastic (p,2p) events with $|p_f| > k_F = 0.220$ GeV/c (the Fermi momentum for ^{12}C), we extract the fraction of these events which also have $|p_n| > k_F$. Finally, in Sect. VI, we present the summary and conclusions.

II. EXPERIMENTAL SETUP

A. The EVA Spectrometer

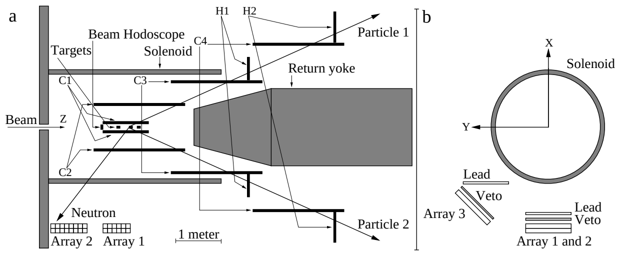

FIG. 1. A schematic side view (a) and a head-on view (b) of the EVA spectrometer and neutron detector arrays.

The EVA spectrometer, shown in Fig. 1, consists of four concentric cylinders of straw-tube drift chambers (C1, C2, C3 and C4) and a solenoidal magnetic field produced by a super-conducting magnet operated at 0.8 T. The solenoid is 2 m in diameter and 3.35 m long. Two scintillator hodoscopes (H1 and H2) are used for additional tracking and for the "level 1" trigger. Wu et al. [12] give the details of the trigger system. Three solid targets, spaced $\sim$ 20 cm apart, were placed on the central axis of the spectrometer. We used either three C targets, or two C targets and one CH_2 target. The targets were 5.1 x 5.1 cm^2 in area and 6.6 cm long in the z direction. Track reconstruction was sufficient to identify the three targets. We will use a right-handed coordinate system to describe the spectrometer. The beam was incident along the z axis, which is the central axis of EVA. The laboratory vertical direction is the x axis, and "beam right" is the y axis.

Beams of 5.9, 8.0 and 9.0 GeV/c were incident along the z axis. Pion contamination of the beam was identified by a pair of differential gas Čerenkov detectors. The rejection efficiency for pions was greater than 99%. Typical beam intensities were 10^7 particles in a one second spill, every three seconds.

B. The Neutron Detectors

The neutron detectors were deployed in three arrays as shown in Fig. 2. All 36 detectors were bars of plastic scintillator with a photo-multiplier tube (PMT) coupled to each end via a tapered acrylic-plastic light pipe. Array 1 consisted of 12 scintillator bars of dimensions 1 m$\times$10 cm$\times$12.5 cm (vertical thickness) arranged in a double layer. The PMTs were 5.1 cm diameter RCA 8575 tubes. The 16 detectors in Array 2 were identical to those in Array 1; Array 2 was also a double layer of detectors. Arrays 1 and 2 were centered around x = -220 cm and y = 0 ($\phi = 180°$). Array 3 consisted of 8 scintillator bars of dimensions 1 m$\times$25 cm$\times$10 cm, with 12.5 cm diameter Hamamatsu R1250 PMTs. These detectors were centered at $\phi = 135°$ at a radial distance of 248 cm from the z axis for the center of their faces.

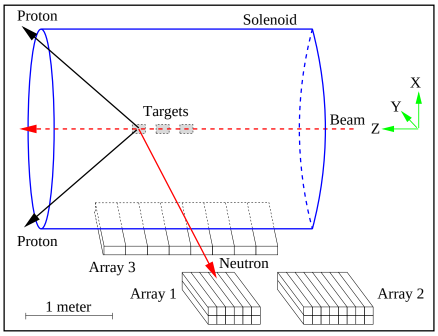

FIG. 2. Schematic arrangement of the neutron detector arrays and the targets, along with the geometry of a typical event.

Between each neutron detector array and the target, we deployed thin "veto" scintillators (0.5 or 1 cm thick) to identify charged particles. Between each veto counter and the targets we placed 1.7 radiation lengths of Pb to reduce the photon flux from the target to acceptable levels. Pulse-height thresholds were set for each PMT on each detector with a ^{60}Co γ-ray source placed near the center of the detector. The threshold was set at the Compton peak from the 1.17 and 1.33 MeV γ-rays, which corresponds closely to 1 MeVee (MeV, equivalent electron). The threshold uncertainty is estimated to be $\pm$ 10%. We determined the neutron-detection efficiencies by the Monte-Carlo method described in Ref. [13]. The efficiencies depend on the neutron momentum and ranged from about 30% near 0.15 GeV/c to about 15% at 0.5 GeV/c, for a typical single counter. We calculated the fraction of the neutrons lost to absorption along their flight paths from the target to the counters by assuming that the removal cross section was equal to the non-elastic cross sections in the materials along these paths [14]. We assigned an uncertainty of 25% to these removal cross sections. The attenuation values ranged from about 35% at the low momenta to about 20% at the high momenta.

The timing signals derived from the two PMTs on each neutron detector were combined in software to produce a position-independent "mean time" for each event, and the position of interaction along the long axis of detector. The time reference for these signals was derived from a "timer" scintillator hodoscope $\sim$ 6 m upstream from the targets. From the mean time, position and (possible) veto signals for each event, we constructed "inverse velocity" (v^{-1}) spectra for both charged and neutral particles detected in each neutron detector.

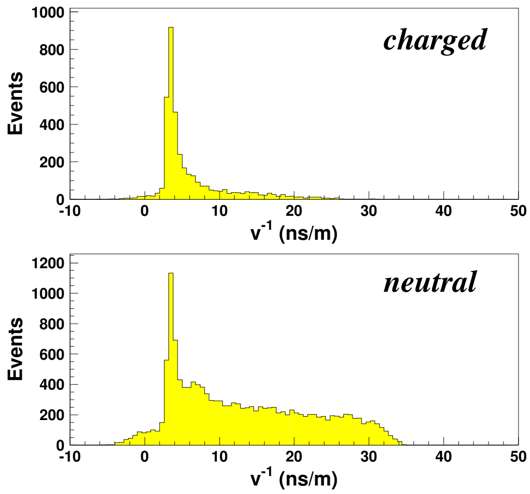

FIG. 3. Inverse velocity spectra for charged and neutral particles detected in neutron detector array 3 for the ^{12}C(p,2p+X) reaction at 5.9 GeV/c beam momentum.

Figure 3 shows typical v^{-1} spectra for charged and neutral particles detected in Array 3 with 5.9 GeV/c protons incident on C and CH_2 targets. Note the prominent γ peak at v^{-1} = 3.3 ns/m in both spectra. The γ peak in the charged-particle spectrum is due to shower production in the lead converter between each detector array and the target. For $v^{-1} > 3.3$ ns/m, where the charged-particle spectrum is primarily hadronic (π, p), the neutral particle flux reaching the detectors is several time the charged-particle flux. We will presume that this neutral-particle flux consists entirely of neutrons, although it may contain a few percent K_0 longs. The useful region of the neutron spectrum is from v^{-1} = 7 ns/m to v^{-1} = 30 ns/m, which corresponds to neutron momenta between 0.10 GeV/c and 0.55 GeV/c. We also observe neutrons in the range $30 \leq v^{-1} \leq 35$ (0.05 GeV/c to 0.10 GeV/c). For these events the scintillation light produced is close to our 1 MeVee threshold, and the detection efficiency cannot be calculated reliably.

A significant fraction ($\sim$ 20%) of the events with neutrons, had neutron signals in two or more scintillator bars. Of these, the large majority had signals in adjacent detectors, suggesting that a single neutron produced a charged particle that passed through both the detector where the neutron interacted, and the adjacent detector. We analyzed these events using the center of the interface (or the corner) between the bars to determine the flight path. If the signals from these two detectors then had velocities within 20% of each other, we retained the event as a "good" neutron and used the average velocity to determine its momentum.

C. Acceptance

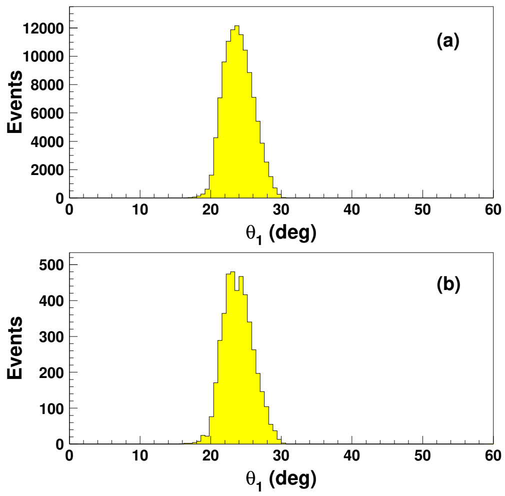

FIG. 4. The distributions of the polar angle θ_1 (for the smaller-angle proton) for (a) ^{12}C(p,2p) and (b) ^{12}C(p,2p+n) events at 5.9 GeV/c beam momentum.

EVA was designed to cover the range of laboratory scattering angles for p-p elastic and quasi-elastic scattering near $\theta_{c.m.} = 90°$. Figure 4 presents plots of θ_1, the angle of the more forward track, for accepted events. The top panel in Fig. 4 is the θ_1 spectrum for events with two, and only two, positively-charged high-transverse-momentum ($\mathbf{p}_t$) tracks. The bottom panel is the θ_1 spectrum with the added constraint that there be a coincident neutron with $0.05 \leq p_n \leq 0.55$ GeV/c. Figure 5 presents spectra of θ_2, the angle for the larger angle track, for the same conditions as the θ_1 spectra in Fig. 4. Note that θ_2 is typically only 3° larger than θ_1.

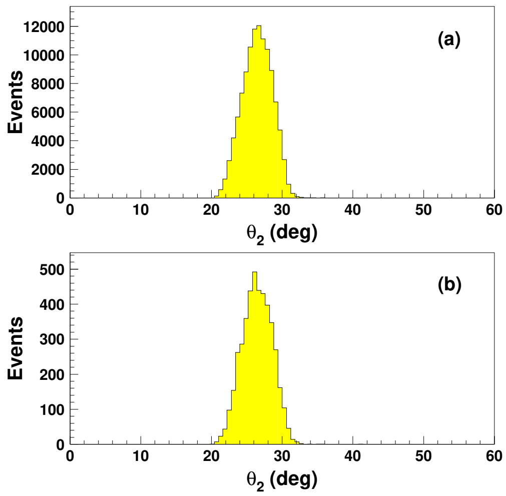

FIG. 5. The distributions of the polar angle θ_2 (for the smaller-angle proton) for (a) ^{12}C(p,2p) and (b) ^{12}C(p,2p+n) events at 5.9 GeV/c beam momentum.

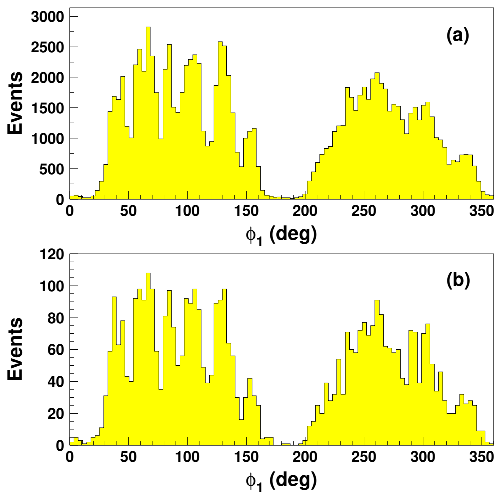

FIG. 6. Distributions of the azimuthal angle ϕ_1 (for the smaller-angle proton) for (a) ^{12}C(p,2p) and (b) ^{12}C(p,2p+n) events at 5.9 GeV/c beam momentum.

Figure 6 is the spectrum of ϕ_1 for the same data set and cuts as Fig. 4. Note the gaps in ϕ coverage around π and 2π due to support structures for the straw-tube drift chambers. Spectra for ϕ_2 show identical patterns. The structure in the distributions is caused by mechanical supports around 0° and 180°, and by inefficiencies in some of the straw tube bundles.

In Fig. 4, Fig. 5 and Fig. 6, the distributions of θ_1, θ_2 and ϕ_1 with the coincident neutron are identical in shape to those without, indicating that there is no reaction bias in the acceptance of EVA for events with coincident neutrons compared to those without.

D. Resolution in $\mathbf{p}_f$

A central aspect of this experiment is our ability to reconstruct "$\mathbf{p}_f$", the momentum of the struck proton in the ^{12}C nucleus before the quasi-elastic p-p collision. The performance of EVA is central to this reconstruction. The "missing energy" (E_{miss}) is defined as

$$E_{miss} = E_{beam} + m - E_1 - E_2 \tag{2}$$

where E_{beam}, E_1 and E_2 are the total energies of the incoming and outgoing particles and m is the nucleon mass in GeV. Figure 7 is the E_{miss} spectrum from CH_2 and C targets bombarded by 5.9 GeV/c protons. The data "cuts" for Fig. 7 are that there should be two, and only two positively-charged high $\mathbf{p}_t$ tracks in EVA. From the clear peak in the CH_2 spectrum for free p-p scattering and comparison of the E_{miss} spectra for C and CH_2 targets we have chosen to make the cut $-0.2 \leq E_{miss}$ (GeV) ≤ 0.8. This should reasonably encompass all quasi-elastic (p,2p) events, since proton separation energies for ^{12}C are typically $\ll 0.2$ GeV.

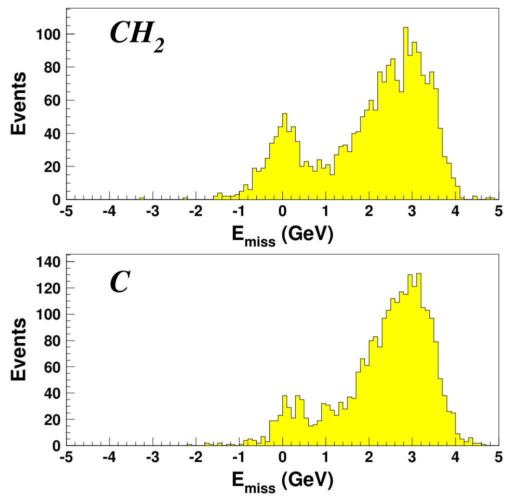

FIG. 7. The missing energy, E_{miss}, distribution for the (p,2p) reaction on CH_2 (upper panel) and C (lower panel) targets bombarded by 5.9 GeV/c protons.

For the CH_2 targets, selecting a predominantly p-p elastic signal by making the indicated cut above ($-0.2 \leq E_{miss}$ (GeV) ≤ 0.8), we can study the resolution of EVA for $\mathbf{p}_f$, since $\mathbf{p}_f \equiv 0$ for p-p elastic scattering. Figure 8 and 9 are plots of $p_{fx'}$ and $p_{fy'}$ for C and CH_2 targets at 5.9 GeV/c beam momentum. The x′ and y′ coordinates are in the plane formed by $\mathbf{p}_0$ and $\mathbf{p}_1$ and normal to that plane, respectively, where $\mathbf{p}_1$ is the momentum of the more forward proton track. For both figures, the spectra for the C target (lower panel) was fit first with a Gaussian centered at 0. Then the spectrum for the CH_2 target (upper panel) was fit with a sum of Gaussians, the first fixed to the shape of the fit to the carbon spectrum and the second (for H) free to vary. The shape for the second Gaussian then gives the resolution, since $p_{fx'}$ and $p_{fy'}$ must be zero for H. The out-of-plane ($p_{y'}$) resulotion (0.039 GeV/c) is substantially better than the in-plane ($p_{x'}$) resolution (0.128 GeV/c). This occurs because $p_{fy'}$ is determined primarily from the non-coplanarity of the event, whereas $p_{fx'}$ is determined primarily by the difference between $\mathbf{p}_1$ and $\mathbf{p}_2$, which are both large relative to $p_{fx'}$.

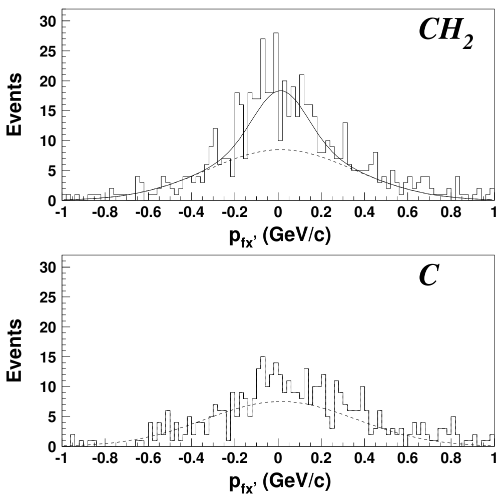

FIG. 8. Plots of $p_{fx'}$, the transverse component of $\mathbf{p}_f$ in the reaction plane, for CH_2 and C targets at 5.9 GeV/c beam momentum. The dashed line in the lower panel is a Gaussian fit to the data for pure C targets. In the upper panel for CH_2, the solid line is a two-Gaussian fit, where broader Gaussian (dashed line) has the shape from the fit to C in the lower panel.

For nuclear reactions at high energy, the natural variables for representing the motion of a nucleon in the nucleus are the light-cone variables ($\mathbf{p}_t$, α). The transverse momentum $\mathbf{p}_t$ can be resolved into the $p_{fx'}$ and $p_{fy'}$ components discussed above, and the variable α, defined as

$$\alpha = \frac{E - p_z}{m} \tag{3}$$

represents the fraction of the nuclear momentum carried by the target nucleon in the light-cone frame. Note that $\alpha = 1$ when p_z is 0.

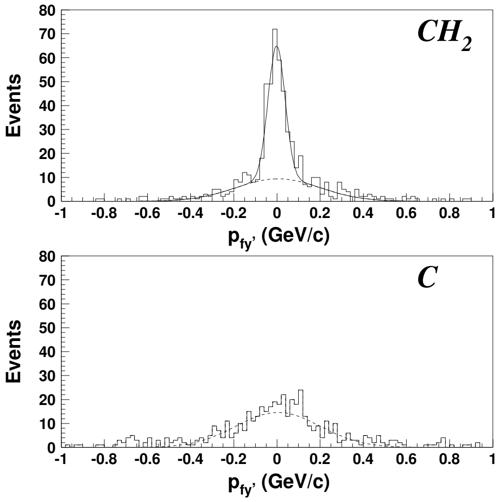

FIG. 9. Plots of $p_{fy'}$, the transverse component of $\mathbf{p}_f$ normal to the reaction plane, for CH_2 and C targets at 5.9 GeV/c beam momentum. The dashed line in the lower panel is a Gaussian fit to the data for pure C targets. In the upper panel for CH_2, the solid line is a two-Gaussian fit, where broader Gaussian (dashed line) has the shape from the fit to C in the lower panel.

The component of $\mathbf{p}_f$ in the z direction, p_{fz}, is relatively poorly defined when compared with p_{fx} and p_{fy} (or $p_{fx'}$ and $p_{fy'}$), because it results from the subtraction of two large numbers (p_{1z} and p_{2z}) from another large number, p_0. This results in a large uncertainty in p_{fz} (close to ± 0.4 GeV/c) when computed as $p_{1z} + p_{2z} - p_0$. Because α in Eqn. (3) involves $E - p_z$, there is a natural uncertainty compensation resulting from the subtraction of p_z from E.

In Figure 10 we present fits to α spectra for C and CH_2 targets similar to those for $p_{fx'}$ and $p_{fy'}$ presented in Figs 8 and 9. From Fig. 10 we see that the resolution in α is ± 0.040. We can then invert Eqn. (3), and make the approximation that $E \approx m$ to obtain

$$p_{fz} = m(1 - \alpha) \tag{4}$$

The resolution in p_{fz} calculated with Eqn. (4) is then $\Delta p_{fz} = m\Delta\alpha = 0.038$ GeV/c, an order of magnitude reduction in the uncertainty.

So in summary our resoluton in $\vec{p_f}$ is

$$\Delta p_{fx'} = 0.124 GeV/c$$
$$\Delta p_{fy'} = 0.039 GeV/c$$
$$\Delta p_{fz'} = 0.038 GeV/c$$

Note in Fig. 10 that the spectrum of α for ^{12}C is peaked near $\alpha = 0.95$ not $\alpha = 1$. This is indicative of the preferential selecion of nuclear protons with p_f in the beam direction ($\alpha < 1$) due to the s^{-10} dependence of $\frac{d\sigma}{dt}$ for p-p scattering near 90° c.m.

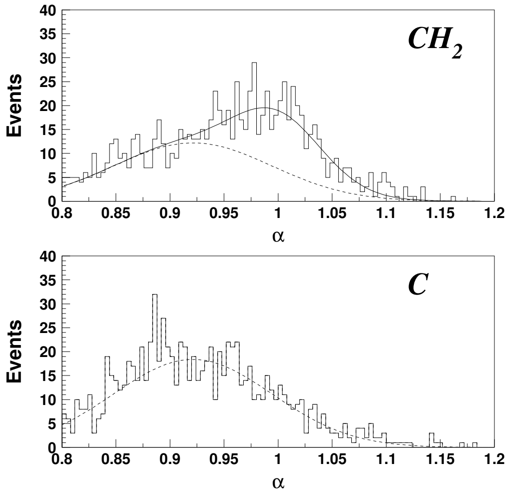

FIG. 10. Plots of the light-cone variable α for CH_2 and C targets at 5.9 GeV/c beam momentum. The dashed line in the lower panel is a Gaussian fit to the data for pure C targets. In the upper panel for CH_2, the solid line is a two-Gaussian fit, where broader Gaussian (dashed line) has the shape from the fit to C in the lower panel.

III. TRIPLE COINCIDENCE RESULTS

For all of the results discussed below we applied the five following cuts to the data:

(1). The projectile should be a proton, as determined by Čerenkov detectors in the beam.

(2). There should be two (and only two) high-$\mathbf{p}_t$ (> 0.6 GeV/c) positive-charge tracks.

(3). The missing energy, E_{miss} should be appropriate for quasi-elastic scattering, and was defined by the resolution at each energy [1].

(4). The neutron momentum should be in the range: $0.05 < p_n < 0.55$ GeV/c.

(5). The laboratory azimuthal angles for the two detected protons must lie within $\pm$ 45° of the plane through EVA parallel to the face of the active neutron detector.

Cut (5) was implemented so that we could combine our results with those in [2], which were also taken with EVA but with more limited acceptance.

A. Directional Correlations

Our primary objective was to identify short-range correlated n-p pairs in ^{12}C nuclei. The signature of such pairs is that the momentum of the detected neutron, $\mathbf{p}_n$ $\approx -\mathbf{p}_f$. We note, however, that the motion of the c.m. of such an n-p pair in the nucleus will keep this from being a perfect equality. Because the resolution for $\mathbf{p}_n$ (a "directly-measured" quantity) is much better than the resolution for $\mathbf{p}_f$ (a "reconstructed" quantity), we will use p_n as our primary variable for most of the results reported below.

B. One-Dimensional Correlation

The simplest directional correlation we can construct is "up-down". The neutron detectors were all placed below the mid-plane of EVA, so the neutrons were all detected in the "downward" direction. We can then compare this with the "upward" component of $\mathbf{p}_f$.

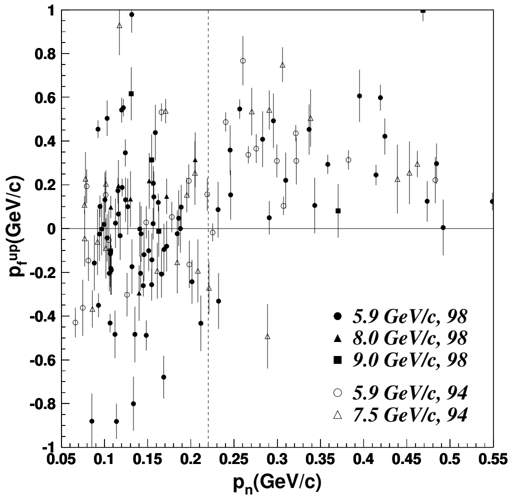

FIG. 11. Scatter plot of p_f^{up} vs. p_n with cuts 1, 2, 3, 4 and 5 (see text) for ^{12}C(p,2p+n) events. Data labelled "98" (solid symbols) are for this work. Data labelled "94" are from Aclander, et al. (Ref. [2]). The vertical dashed line at 0.22 GeV/c corresponds to k_F, the Fermi momentum for ^{12}C.

Figure 11 is a scatter plot for (p,2p+n) events of p_f^{up} vs. the neutron momentum p_n, where p_f^{up} is the projection of $\mathbf{p}_f$ on an axis normal to the faces of the neutron detectors. The vertical dashed line in Fig. 11 is at k_F = 0.22 GeV/c, the Fermi momentum for ^{12}C [15]. The experimental uncertainties in Fig. 11 are derived from resolutions measured for p-p elastic scattering. We note in Fig. 11, that there is a striking difference in the distribution of p_f^{up} for $p_n < k_F$ and $p_n \geq k_F$. For $p_n < k_F$ the events are distributed nearly equally between those with $p_f^{up} > 0$ ("up") and $p_f^{up} < 0$ ("down"). By contrast, for $p_n \geq k_F$, a large fraction of the events have $p_f^{up} >$ 0. Thus $\mathbf{p}_f$ is predominantly "up" when $\mathbf{p}_n$ is (by definition) "down" for $p_n \geq k_F$. This is a strong confirmation of what was reported by Aclander et al. in [2].

C. Transverse Correlations

The next level of correlation we wish to examine is directional correlation in the two-dimensional "transverse" (x-y) plane. We define the transverse momentum vectors:

$$\mathbf{p_{nt}} = (p_{nx}, p_{ny}),$$
$$\mathbf{p_{ft}} = (p_{fx}, p_{fy}).$$

Then if we call the angle between $\mathbf{p}_{nt}$ and $\mathbf{p}_{ft}$ β:

$$\beta = \cos^{-1}\left(\frac{\mathbf{p}_{nt} \cdot \mathbf{p}_{ft}}{|\mathbf{p}_{nt}||\mathbf{p}_{ft}|}\right). \tag{5}$$

Figures 12a and 12b are plots of β for our data with cuts 1-5 combined with the data of Ref [2]; 12a is for $|\mathrm{p}_n| > \mathrm{k}_F$, 12b is for $|\mathrm{p}_n| < \mathrm{k}_F$. In 12a we see again a strong directional correlation between $\mathbf{p}_{nt}$ and $\mathbf{p}_{ft}$ with almost all events having $\beta > 90°$, whereas for $|\mathrm{p}_n| < \mathrm{k}_F$ the distribution is flat, to within statistics.

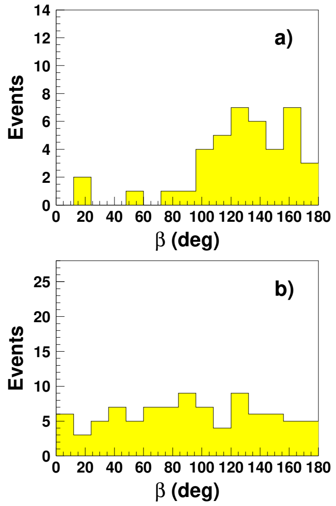

FIG. 12. Plots of β, the angle in the transverse plane between $\mathbf{p}_f$ and $\mathbf{p}_n$. Panel (a) is for events with $\mathrm{p}_n > 0.22$ GeV/c, and panel (b) is for events with $\mathrm{p}_n < 0.22$ GeV/c, where 0.22 GeV/c = k_F, the Fermi momentum for ^{12}C.

D. The Longitudinal Correlation

As noted in Sect. II.D, the uncertainty for the longitudinal component of $\mathbf{p}_f$ is rather large ($\sim$ 0.40 GeV/c) if computed directly from $\mathbf{p}_0$, $\mathbf{p}_1$ and $\mathbf{p}_2$. Thus we consider instead the light cone variable α = (E- p_z)/m. For a correlated n-p pair in the nucleus with $\mathbf{p}_n \approx$ -$\mathbf{p}_f$, we would expect $\alpha_n + \alpha_p \approx 2$, where α_p = (E-p_{fz})/m.

As noted in the introduction to this paper, the pp cross section, $\frac{d\sigma}{dt}$, near 90° c.m. is proportional to s^{-10}. We therefore need to correct for this "reaction bias" when looking at longitudinal variables. The differential cross section as a function of the solid angle, $\frac{d\sigma}{d\Omega}$, is related to $\frac{d\sigma}{dt}$ by:

$$\frac{d\sigma}{dt} = \frac{4\pi}{(s - 4m^2)}\frac{d\sigma}{d\Omega} \tag{6}$$

Therefore, for large s, $\frac{d\sigma}{d\Omega}$ is approximately proportional to s^{-9}, and this stong s-dependence enhances quasielastic reactions with low s for the p-p collisions. Protons in the nucleus with longitudinal momentum in the same direciton as the beam are thus more likely to be knocked out. We therefore weighted each event by a correction factor equal to $(s/s_0)^9$, to obtain the nuclear distributions without the reaction bias, where s_0 is the total c.m. energy for pp$\rightarrow$pp at each beam momentum, and s is calculated for each event from $\mathbf{p}_f$ for that event.

In Fig. 13 we show plots of α_p, α_n and $\alpha_p + \alpha_n$ (all with s-weighting) for events with $\mathrm{p}_n > \mathrm{k}_F$. We note for Fig. 13 that α_p (for the proton) is generally < 1 and $\alpha_n > 1$. Of couse, our placement of the neutron detectors primarily in the backward hemisphere forces α_n to be largely > 1. However, as we saw in Fig. 10, α_p is usually < 1 without the requirement of a coincident neutron, because of the s^{-10} dependence of p-p scattering near 90° c.m. In Fig. 13, with $\mathrm{p}_n > \mathrm{k}_F$, we see that the α_p distribution peaks at $\sim$ 0.85 in contrast with the peak at 0.94 in Fig. 10. This is even more striking when we consider that the data in Fig. 10 have not been "s-weighted", an operation which shifts the α_p spectrum towards 1. We see also that the $\alpha_p + \alpha_n$ spectrum indeed peaks at $\sim$ 2 as we would expect for $\mathbf{p}_n \approx \mathbf{p}_f$.

In Fig. 13, the spread of $\alpha_n + \alpha_p$ about 2 should be due to the c.m. motion of the pair. Ciofi degli Atti *et al.* [16] emphasized the importance of the c.m. motion of correlated pairs for explaining nucleon spectral functions at large momenta and removal energies.

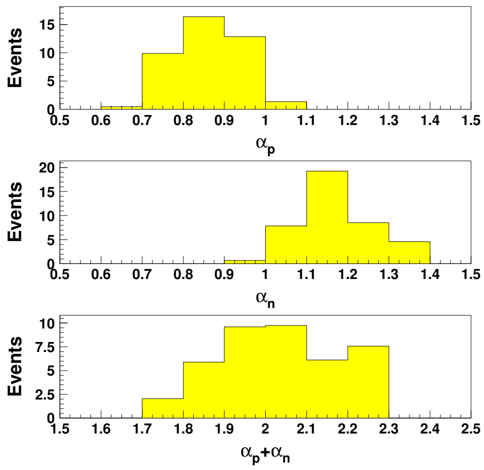

FIG. 13. Plots of the light-cone variables α_p, α_n, and their sum $\alpha_p + \alpha_n$ for events with $\mathrm{p}_n > \mathrm{k}_F = 0.22$ GeV/c. Data are for ^{12}C(p,2p+n) events. Each event has been "s-weighted", as described in the text.

E. The Full Correlation

We now construct the full directional correlation between $\mathbf{p}_f$ and $\mathbf{p}_n$ as

$$cos\gamma = \frac{\mathbf{p_f} \cdot \mathbf{p_n}}{\mid \mathbf{p_f} \mid\mid \mathbf{p_n} \mid} \tag{7}$$

where γ is the angle between $\mathbf{p}_f$ and $\mathbf{p}_n$.

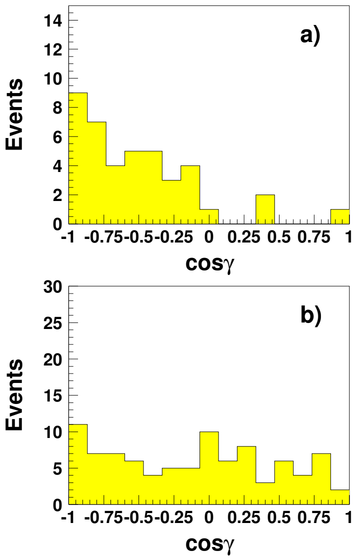

FIG. 14. Plots of cosγ, where γ is the angle between $\mathbf{p}_n$ and $\mathbf{p}_f$, for ^{12}C(p,2p+n) events. Panel (a) is for events with $p_n > 0.22$ GeV/c, and panel (b) is for events with $p_n < 0.22$ GeV/c; 0.22 GeV/c = k_F, the Fermi momentum for ^{12}C.

In Fig. 14a and 14b we plot cosγ for $p_n \geq k_F = 0.22$ GeV/c and $p_n < k_F$, respectively. As in Fig. 11 there is a pronounced difference between the distributions for $p_n \geq k_F$ and $p_n < k_F$. Fig. 14a shows a strong "back-to-back" directional correlation with the distribution peaking at $\cos\gamma = -1$; only 3 events have $\cos\gamma > 0$. By contrast, in Fig. 14b, the distribution is nearly uniform in cosγ, and the numbers of events for $\cos\gamma < 0$ and $\cos\gamma > 0$, are the same within statistics (51 and 43, respectively). For Fig. 14a ($p_n > k_F$), the probability that 38 uncorrelated events could be distributed 35 to 3 is vanishing small ($\sim 10^{-8}$).

To check the results in Fig. 14, we generated background spectra of events with two high p_t tracks plus one soft track in EVA. The resulting spectra for both $p_n > k_F$ and $p_n < k_F$ were small and flat, indicating that the peak at $\cos\gamma = -1$ in Fig. 14a is not an instrumental artifact, and that backgrounds are small. This is indicative of why we are able to identify p-p quasi-elastic scattering, in spite of the poor missing-energy resolution (Fig. 7). EVA provides nearly 4π coverage for charged particles, with multi-track capabilities. We require two nearly coplanar, positively-charged high-$\mathbf{p}_t$ tracks, and explicitly reject events with any other charged particle tracks, hard or soft. This then is a very effective filter for p-p quasi-elastic scattering, as seen in [1].

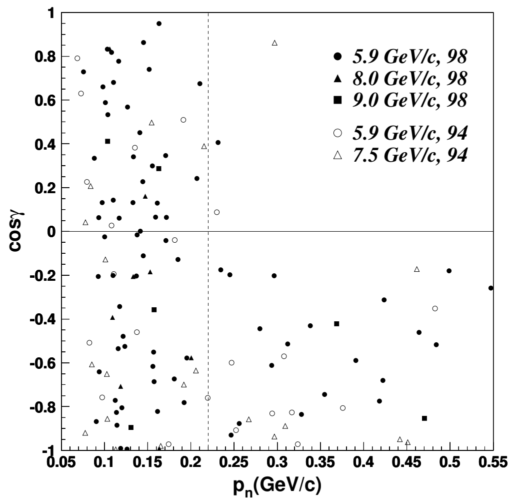

FIG. 15. Scatter plot of cosγ vs. p_n with cuts 1, 2, 3, 4 and 5 (see text) for ^{12}C(p,2p+n) events. Data labelled "98" (solid symbols) are for this work. Data labelled "94" are from Aclander, et al. (Ref. [2]). The vertical dashed line at 0.22 GeV/c corresponds to k_F, the Fermi momentum for ^{12}C.

Figure 15 is a scatter plot for (p, 2p+n) events of cosγ vs. p_n. Again, the vertical dashed line in Fig. 15 is at $k_F = 0.22$ GeV/c. Figure 15 shows the same dramatic difference as Fig. 11 for events with $p_n < k_F$ and events with $p_n > k_F$. For $p_n < k_F$ the events are essentially randomly distributed; for $p_n > k_F$, all but 3 events have $\cos\gamma <$ -0.15, which is a very strong signature of directional correlation between $\mathbf{p}_f$ and $\mathbf{p}_n$.

IV. THE RELATIVE AND C.M. MOTION OF CORRELATED np PAIRS

The effects of initial-state and final-state interactions (ISIs and FSIs) are expected to be larger in the transverse than in the longitudinal direction [17]. Therefore, in extracting the relative and c.m. motion for correlated n-p pairs we focus on the longitudinal (z) components of $\mathbf{p}_n$ and $\mathbf{p}_f$.

In the longitudinal direction:

$$p_z^{cm} = p_{nz} + p_{fz}. \tag{8}$$

By approximating $E_p \approx E_n \approx$ m, we obtain

$$\alpha_p + \alpha_n = (1 - \frac{p_{fz}}{m}) + (1 - \frac{p_{nz}}{m}) \tag{9}$$

which leads to

$$p_z^{cm} = 2m(1 - \frac{\alpha_p + \alpha_n}{2}). \tag{10}$$

The longitudinal momentum of the particles in their c.m. frame can be extracted from the difference of the α variables. By again approximating $E_p \approx E_n \approx$ m, we obtain

$$\alpha_p - \alpha_n = (1 - \frac{p_{fz}}{m}) - (1 - \frac{p_{nz}}{m}) = (\frac{p_{nz} - p_{fz}}{m}), \quad (11)$$

which leads to

$$p_z^{rel} = m|\alpha_p - \alpha_n|. \quad (12)$$

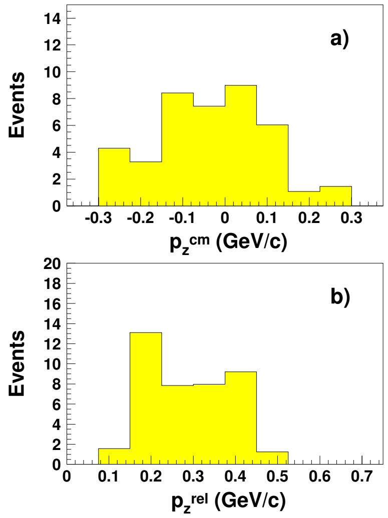

FIG. 16. Plots of (a) p_z^{cm} and (b) p_z^{rel} for correlated n-p pairs in ^{12}C, for ^{12}C(p,2p+n) events. Each event has been "s-weighted", as described in the text.

Figure 16a and 16b are plots of p_z^{cm} and p_z^{rel}. For p_z^{cm} in Fig. 16a, the centroid is -0.013 ± 0.027 GeV/c. The spread in the distribution is $\sigma = 0.143 \pm 0.017$ GeV/c. For p_z^{rel} in Fig. 16b, the centroid is 0.289 ± 0.017 GeV/c, and the width is $\sigma = 0.097 \pm 0.007$ GeV/c.

V. THE "CORRELATED FRACTION" OF (p,2p) EVENTS

An interesting number which can be extracted from our data, is the fraction of ^{12}C(p,2p) events which have correlated neutrons with $\mathbf{p}_n \approx -\mathbf{p}_f$ when p_n, $p_f \geq k_F$. To extract this number, we need to correct the measured neutron flux for neutron detection efficiency and flux attenuation, and for solid-angle coverage. Our neutron detectors were placed almost entirely in the backward hemisphere, so we calculate the fraction of the 2π sr for the backward hemisphere covered by our detectors.

What we then calculated was:

$$F = \frac{\textit{corrected \# of (p,2p+n) events}}{\textit{\# of (p,2p) events}} = \frac{A}{B} \quad (13)$$

for the same data sample. B was obtained by applying cuts (1), (2), (3) and (5), to events with $p_f \geq k_F$ for our 5.9 GeV runs excluding the data reported in [2]. The quantity B = 2205 then was all events satisfying the above cuts and data selection. The quantity A was obtained from the sample of all 18 (p,2p+n) events in the sample B with $p_n \geq k_F$, where a correction for flux attenuation (t) and detection efficiency (ϵ) was applied event-by-event; see Sect. II.B. for details. The resulting quantity was then corrected for the solid-angle coverage to obtain A:

$$A = \frac{2\pi}{\Delta\Omega} \sum_{i=1}^{18} \frac{1}{\epsilon_i} \cdot \frac{1}{t_i} = 1090. \quad (14)$$

The average value of $\epsilon_i^{-1} t_i^{-1}$ was 8.2 ± 0.82 and $2\pi/\Delta\Omega = 7.42$. We then obtain

$$F = \frac{A}{B} = 0.49 \pm 0.13. \quad (15)$$

The sample of 18 measured (p,2p+n) events is clearly small, and the uncertainty in F is determined largely by this sample size. The result is still compelling: roughly half of the measured quasielastic (p,2p) events with $p_f > k_F$ have a neutron emitted in the backward hemisphere with $p_n > k_F$. We note that this result is similar to that reported by Malki, et al. [8] for hard inclusive (p,2p+n).

VI. DISCUSSION AND CONCLUSIONS

In summary, for quasi-elastic (p,2p) events we reconstructed $\mathbf{p}_f$, the momentum of the struck proton in ^{12}C before the reaction. Then, for neutrons with momenta $p_n > 0.220$ GeV/c (which is k_F, the Fermi momentum for ^{12}C), we found a strong directional correlation for $\mathbf{p}_f$ and $\mathbf{p}_n$, namely $\mathbf{p}_n \approx -\mathbf{p}_f$. By contrast, for $p_n < k_F$ we found no correlation. This was evident in the one-dimensional "up-down" and longitudinal correlations and the full three-dimensional directional correlation. For the longitudinal direction, where ISI and FSI effects should be small, we extracted the distributions of c.m. and relative motion for n-p pairs.

We conclude, therefore, that neutrons emitted into the backward hemisphere with $p_n > k_F$ come from n-p SRC, since SRC is a natural mechanism to explain such momentum-correlated pairs. An analysis of the sample of events for 5.9 GeV/c beam momentum with $p_f > k_F$, indicates that $49 \pm 13\%$ of these events have a correlated neutron with $p_n > k_F$. Because this measured fraction includes only n-p and not p-p SRC, the total correlated fraction must be even larger. Therefore we conclude that 2N SRC must be a major source of high-momentum nucleons in nuclei. We also measured the longitudinal components of the c.m. momentum of the correlated pn pair and the relative momentum of the pn pair in its c.m. system.

Further applications of the technique used in this work and in Ref. [2] are planned [18] at the Thomas Jefferson National Accelerator Facility, as experiment E01-015.

The two high-resolution spectrometers in Hall A at Jefferson Laboratory will be used to identify ^{12}C(e,e$'$p) quasi-elastic scattering. Then triple-coincidence protons will be detected with the 100 msr "BigBite" spectrometer, and triple-coincidence neutrons will be detected with an array of 88 large plastic scintillator bars, placed behind "BigBite" and covering the identical solid angle. Thus experiment E01-015 will provide simultaneous information on p-p and p-n SRC.

ACKNOWLEDGMENTS

We are pleased to acknowledge the assistance of the AGS staff in building and rebuilding the detector and supporting the experiment, particularly our liaison engineer C. Pearson, and the continuing support of Drs. D. Lowenstein and P. Pile. This research was supported by the U.S. - Israel Binational Science foundation, the Israel Science Foundation founded by the Israel Academy of Sciences and Humanities, NSF grants No. PHY-9501114, PHY-9722519, PHY-0099387 and the U.S. Department of Energy grant No. DEFG0290ER40553.

---

[1] Y. Mardor *et al.*, Phys. Lett. B **437**, 257 (1998).
[2] J. Aclander *et al.*, Phys. Lett. B **453**, 211 (1999).
[3] L.L. Frankfurt and M.I. Strikman, Phys. Rep. **76**, 214 (1981); Phys. Rep. **160**, 235 (1988).
[4] A. Tang *et al.*, Phys. Rev. Lett. **90**, 042301 (2003).
[5] K.I. Blomqvist *et al.*, Phys. Lett. B **421**, 71 (1998).
[6] C.J.G. Onderwater *et al.*, Phys. Rev. Lett. **81**, 2213 (1998).
[7] R. Starink *et al.*, Phys. Lett. B **474**, 33 (2000).
[8] A. Malki *et al.*, Phys. Rev. C **65**, 015207 (2001).
[9] A. Leksanov *et al.*, Phys. Rev. Lett. **87**, 212301 (2001).
[10] G.R. Farrar *et al.*, Phys. Rev. Lett. **62**, 1095 (1989).
[11] A. De Shalit and H. Feshbach, Theoretical Nuclear Physics, Wiley, 1974.
[12] J.Y. Wu *et al.*, Nucl. Instrum. Methods Phys. Res., Sect. A **349**, 183 (1994).
[13] R.A. Cecil *et al.*, Nucl. Inst. and Meth. **161**, 439 (1979).
[14] D.J. Hughes and R.B. Schwartz, BNL report 325 (1958).
[15] E.J. Moniz *et al.*, Phys. Rev. Lett. **26**, 445 (1971).
[16] C. Ciofi degli Atti, S. Simula, L.L. Frankfurt and M.I. Strikman, Phys. Rev. C **44**, 7 (1991).
[17] L.L. Frankfurt *et al.*, Phys. Rev. C **56**, 1124 (1997).
[18] TJNAF experiment E01-015, E. Piasetzky, W. Bertozzi, J. W. Watson, and S. Wood spokespersons (2001).